JET STRUCTURE IN DEEP-INELASTIC SCATTERING

D. LÜKE

Department of Physics, University Dortmund, D-44221 Dortmund,Germany
E-mail: lueke@physik.uni-dortmund.de

Various jet studies in di-jet production in deep-inelastic scattering are presented. Measured quantities are jet-shapes and multiplicity of sub-jets. Fragmentation measurements have been performed to determine fragmentation functions and particle multiplicities.

1 Introduction

The analysis of hadronic final states in deep-inelastic lepton-proton scattering (DIS) allows to examine the structure of jets of collimated hadrons. In this contribution jet structures of neutral-current DIS-reactions in the Breit-reference frame are presented by the H1 [1, 2]- and the ZEUS [3]-collaboration using data taken at the HERA ep-storage rings in 1994-1997.

2 Internal Jet Structure in Di-jet Production

The internal jet structure in deep-inelastic scattering events has been analyzed using neutral-current di-jet events in the Breit-reference frame.

The ep Breit frame is aligned with the $\gamma^\star p$ center-of-mass frame (where $\gamma^\star = e - e'$ is the exchanged virtual photon in neutral-current reactions), but boosted along the z-direction such that $\gamma^\star$ has zero energy, zero transverse momentum and a z-momentum of $p_z = -Q$ (see Fig.1).

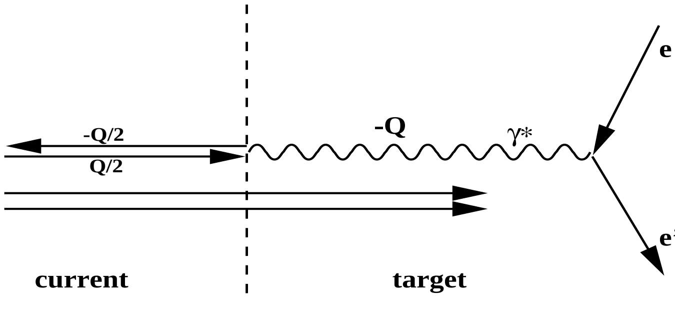

Figure 1: Neutral-current reaction in Breit reference frame

In the naive quark-parton model the quark has a momentum of +Q/2 *before* the interaction with the virtual photon, while its momentum is -Q/2 *after* the interaction. In the Breit frame, the *target*-hemisphere is the hemisphere of *positive* p_z (i.e. in direction of the proton) while the *current*-hemisphere has *negative* p_z (i.e. in direction of the photon).

The data shown in this chapter have been taken by the H1-collaboration in 1994; they correspond to an integrated luminosity of 2 pb^{-1}. Particle jets have been formed using the k_T-cluster-algorithm [4]. Events with $\geq$ 2 jets of transverse energy $E_{T,jet} \geq 5$ GeV in the Breit frame have been selected. The internal jet structure has been determined mainly from jets in the target-hemisphere of the Breit system.

2.1 Jet-Shapes

The observable jet-shape, $\psi(r)$, is defined as the averaged fractional transverse energy E_T of a jet within a subcone of radius r in pseudo-rapidity and azimuth space around the jet axis:

$\psi(r) = \frac{1}{N_{jets}} \sum \rho(r)$ (summed over all selected jets)

with $\rho(r) = \sum E_{T,i} \ / \ E_{T,jet}$

(summed over all particles i within subcone of radius r).

The resolution parameter r is varied between $0 \leq r \leq R$ (where R=1 has been chosen). Fig.2 shows the $\psi(r)$ as a function of r for two different intervals of the transverse jet energy $E_{T,jet,Breit}$ and three different intervals of the pseudo-rapidity η_{Breit}. For a fixed value of the resolution parameter r = 0.5, the jet-shape $\psi(r)$ is given as a function of η_{Breit} in Fig.3 . Wider jets are produced at lower transverse jet energy $E_{T,jet,Breit}$ and at larger pseudo-rapidity η_{Breit}. A possible explanation for this behaviour is that the internal jet structure is influenced by particles produced by QCD radiation near the proton remnant, i.e. at larger η_{Breit}.

Predictions of various QCD-based models: LEPTO [5], HERWIG [6] and ARIADNE [7] are given in Fig.2; they are in fair agreement with the measured jet-shapes. Similar studies on jet-shapes have been presented [8] by the ZEUS-collaboration.

2.2 Multiplicity of Sub-Jets

Internal jet structure can be studied through the multiplicity of sub-jets (N_{subjet}); it is defined as the number of clusters found be the k_T-cluster-algorithm when using a cut-off parameter y_{cut} in the definition of the distance between two particles:

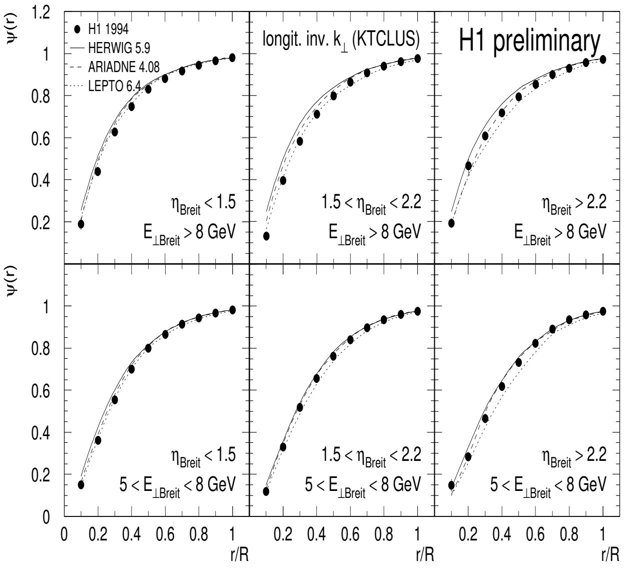

Figure 2: Jet-shape $\psi(r)$ as function of the resolution parameter r, for different intervals of $E_{T,Breit}$ and η_{Breit}

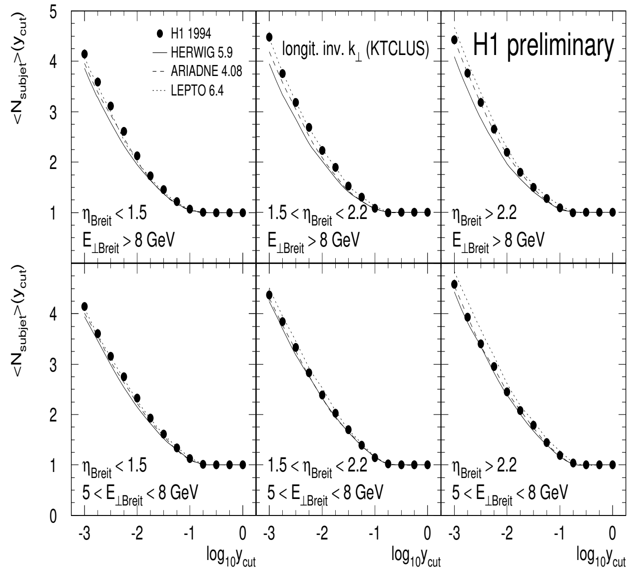

Figure 4: Number of sub-jets as function of the resolution parameter y_{cut}, for different intervals of $E_{T,Breit}$ and η_{Breit}

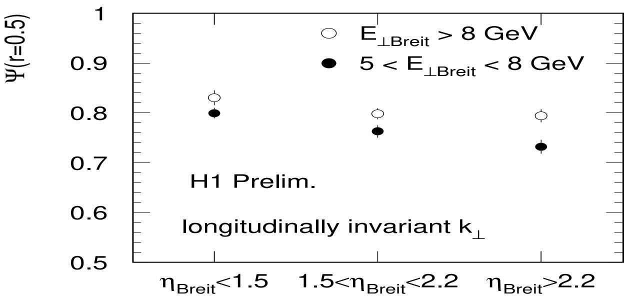

Figure 3: Jet-shape at fixed subcone radius r=0.5, as function of the pseudo-rapidity η_{Breit}

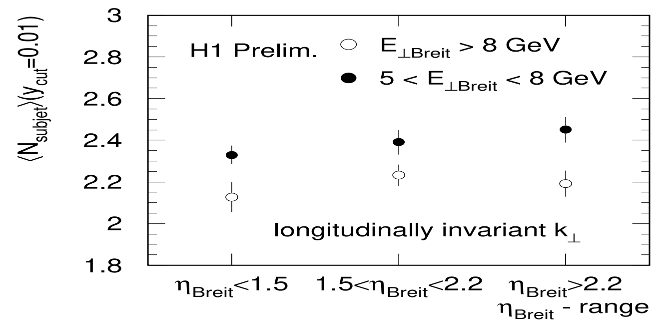

Figure 5: Number of sub-jets at fixed resolution parameter $y_{cut} = 0.01$, as function of the pseudo-rapidity η_{Breit}

for any pair of particles i,j within a sub-jet their distance has to be smaller than y_{cut}:
$distance_{ij} = \frac{(\Delta\eta^2+\Delta\phi^2)}{R_o^2} \star \frac{min(\ E_{T,i}^2\ ,\ E_{T,j}^2\ )}{E_{T,jet}^2} \leq y_{cut}$.
By definition, $N_{subjet} \to 1$ if the resolution parameter y_{cut} approaches its maximum value, $y_{cut} = 1$.

Fig.4 shows the sub-jet multiplicity as a function of the resolution parameter y_{cut} for two intervals of the transverse jet-energy $E_{T,jet,Breit}$ and three different intervals of the pseudo-rapidity η_{Breit}. For a fixed value of $y_{cut} = 0.01$, the sub-jet multiplicity is shown as function of η_{Breit} in Fig.5 The number of sub-jets increases with decreasing transverse jet-energy $E_{T,jet,Breit}$ and increasing pseudo-rapidity η_{Breit}. The predictions from QCD-based models LEPTO, HERWIG and ARIADNE, shown in Fig.4, are in fair agreement with the measured sub-jet multiplicity.

3 Fragmentation measurements in DIS

3.1 Fragmentation Functions

The fragmentation functions presented here have been measured by the H1-collaboration (using data from 1996 with an integrated luminosity of 7 pb^{-1}), and by the ZEUS-collaboration (using data from 1994-1997 with an integrated luminosity of 38 pb^{-1}).

The fragmentation functions shown in Fig.6 are the scaled momentum distributions of single particles in the *current*-hemisphere of the Breit reference frame: $\frac{1}{N_{evts}} \cdot \frac{dn}{dx_p}$ with $x_p = p^{Breit}\ /\ p_{max}^{Breit}$
where the maximum possible momentum has been set to

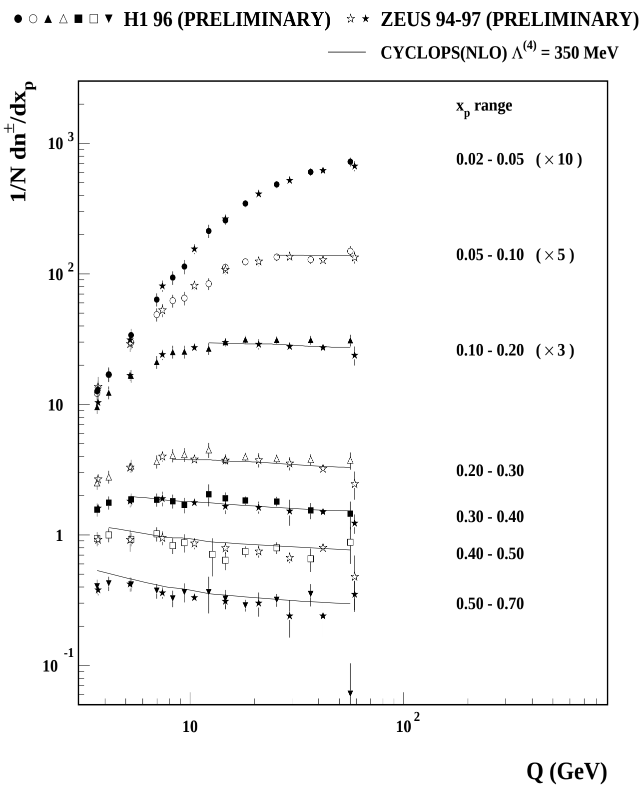

Figure 6: Fragmentation function as a function of Q

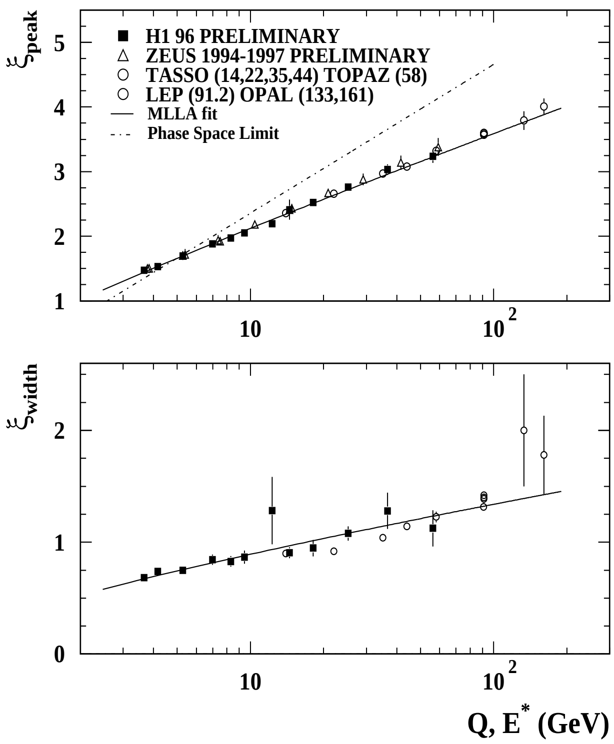

Figure 7: Peak and width of fragmentation function as a function of Q (for ep data) resp. $E^\star$ (for e^+e^- data)

its phase-space limit in the Breit frame: $p_{max}^{Breit} = Q/2$. In Fig.6 the fragmentation functions are plotted as function of Q for different intervals of the scaled momentum x_p. Clear scaling violations are shown: at smaller x_p they strongly rise with increasing Q, and at larger x_p they slowly drop with increasing Q. This behaviour can be seen in both, the H1-data and the ZEUS-data. The solid curves in Fig.6 are from a *next-to-leading-order* (NLO) calculation [9]; they are in good agreement with the measured data in the kinematic range of larger x_p and larger Q, where the calculation is *infrared-safe.*

The first and second moments of the fragmentation function are its peak and its width; both can be determined from the density distribution of the variable $\xi = ln(1/x_p)$ through a simple Gaussian fit, because dN/dξ has a Gaussian shape near its peak (see Ref.10).

Fig.7 shows peak and width of the ξ-distribution as function of Q for the H1 and ZEUS data. Both observables ξ_{peak} and ξ_{width} show a linear rise with Q. The ep-data, plotted against Q, are compared with ξ_{peak} and ξ_{width} from various e^+e^- experiments, where the relevant evolution variable is the e^+e^- center-of-mass energy $E^\star$. Obviously the fragmentation functions for ep processes (when measured in the current region of the Breit reference frame) and for e^+e^- processes show the same behaviour - supporting the idea of "process independence of fragmentation".

The solid curves in Fig.7 represent the expectations $\xi_{peak} \propto ln\ Q + const$ and $\xi_{width} \propto (ln\ Q)^{3/4}$ derived from Modified-Leading-Log-Approximation (MLLA) [10]; these calculations are in good agreement with the measured values.

3.2 Averaged Charged Multiplicity

The averaged charged multiplicity of deep-inelastic scattering events, as presented here, has been determined only from charged particles in the *current*-hemisphere of the Breit reference frame. This restriction in phase space allows for a comparison with e^+e^- data.

Fig.8 shows the averaged charged multiplicity <n> as function of Q for ep data from H1 and ZEUS. Contributions from K^o and Λ decays have been subtracted. A strong rise of <n> with increasing Q is observed. For comparison, the averaged charged multiplicity for e^+e^- is shown as function of the e^+e^- center-of-mass energy $E^\star$ (solid curve) according to a parametrization [11] of data from various e^+e^- experiments. Also these multiplicity values for e^+e^- have been corrected for K^o and Λ decays. To correspond to the fragmentation of only *one* quark, the <n> values for e^+e^- have been halved for the comparison with ep. At smaller values of $Q < 10\ GeV$, the ep data show a shortfall which can be attributed to higher order QCD-diagrams (like photon-gluon-fusion and QCD-compton) which result in a smaller averaged charged multiplicity in the current hemisphere, and which are not present in e^+e^- interactions. At larger values of $Q > 10\ GeV$, ep and e^+e^- data show the same averaged charged multiplicity, again giving support for the process independence of fragmentation.

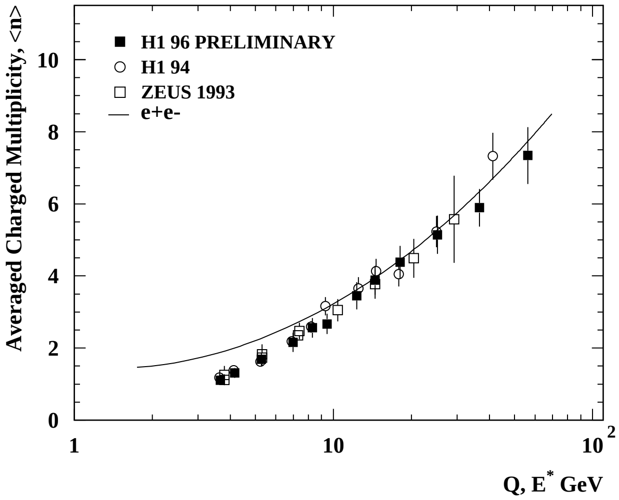

Figure 8: Averaged charged multiplicity as a function of Q (for ep data) resp. $E^\star$ (for e^+e^- data)

4 Summary

Internal jet structure in deep-inelastic scattering has been presented in terms of jet-shapes and multiplicity of sub-jets, determined in the Breit reference frame. The results can be described by QCD-based models. Fragmentation functions and charged particle multiplicities for DIS-events have been studied in the current hemisphere of the Breit frame. They agree with data from e^+e^- experiments and thus support the idea of process independence of fragmentation.

Acknowledgment

I wish to thank my colleagues from H1 and ZEUS who helped me in preparing my talk.
This work has been supported by the Bundesministerium für Bildung, Wissenschaft, Forschung und Technologie, Germany, under contract number 057DO55P.

References

1. H1 Collaboration, paper 532, Contribution to the XXIX International Conference on High Energy Physics, July 1998, Vancouver, BC, Canada
2. H1 Collaboration, paper 531, Contribution to the XXIX International Conference on High Energy Physics, July 1998, Vancouver, BC, Canada
3. ZEUS Collaboration, paper 809, Contribution to the XXIX International Conference on High Energy Physics, July 1998, Vancouver, BC, Canada
4. S.D. Ellis and D.E. Soper, *Phys. Rev.* D **48**, 3160 (1993),
   S. Catani, Yu.L. Dokshitzer, M.H. Seymour and B.R. Webber,*Nucl. Phys.* B **406**, 187 (1993)
5. G. Ingelman, A.Edin and J. Rathsman, *Comp. Phys. Comm.* **101**, 108 (1997)
6. G. Marchinesi et al., *Comp. Phys. Comm.* **67**, 465 (1992)
7. B.R. Webber, *Nucl. Phys.* B **238**, 492 (1984)
8. M. Weber, 33rd Rencontres de Moriond, QCD and High Energy Hadronic Interactions, March 1998, Les Arcs, France
9. D. Graudenz, CERN TH/96-52, CERN TH/96-187 (hep-ph/9610287), CERN TH/96-155 (hep-ph/9606460), PSI-PR/97-20
10. Yu.L. Dokshitzer, V.A. Khoze, A.H. Mueller and S.I. Troyan, "Basics of Perturbative QCD", Editions Frontières (1991), and references therein.
11. OPAL Collaboration, P.B. Acton et al.,*Z. Phys.* C **53**, 539 (1992)